

A highly tunable dynamic thoracic model for Electrical Impedance Tomography

Christos Dimas, Konstantinos Asimakopoulos and Paul P. Sotiriadis

Department of Electrical and Computer Engineering

National Technical University of Athens, Greece

E-mail: chdim@central.ntua.gr, koassim@gmail.com, pps@ieee.org

Abstract—A time-dependent, flexible, 2-dimensional fine thoracic Finite-Element model for continuous lung Electrical Impedance Tomography (EIT) imaging is presented. It can be used as a tool to identify lung EIT hardware specifications, such as minimum frame rate, number of electrodes and noise requirements, as well as for prior evaluation of EIT reconstruction algorithms, before applying in-vivo data. The model is parameterized with respect to electrodes' characteristics, the measuring protocol, structural and temporal properties of the thoracic tissues. It is implemented in FEMM using a script generated by MATLAB code, while the measurements are acquired also by MATLAB. The electrodes' contact impedances, as well as the changes in electrical and geometric properties of the thoracic tissues due to breathing and perfusion, during each particular measuring frame, are taken into account.

Index Terms—Electrical Impedance Tomography, dynamic thoracic model, lungs, breath, circulation, F.E.M., measurement

I. INTRODUCTION

Electrical Impedance Tomography (EIT) is a radiation-free, non-invasive and fast medical imaging technique, in which a small amplitude, medium frequency (kHz) and safety-standard current is applied through an electrode array in the under examination domain. From the raw voltages acquired, a conductivity distribution map of the subject's interior is estimated. EIT is safer, faster and cheaper than Computed Tomography (CT) or Magnetic Resonance Imaging (MRI), while offering portability and exceptional temporal resolution. This makes EIT sufficient for continuous monitoring applications, such as real-time lung imaging of patients with respiratory failure, that require mechanical ventilation, or neonates that should never be subjected to any ionizing radiation [1], [2]

Despite its remarkable capabilities in applications that require sufficient temporal resolution, EIT lacks adequate spatial resolution and robustness in noisy measurements. Therefore, carefully designed and high quality performance hardware systems are deployed in order to achieve high SNR level bio-signals. Over the last 40 years of EIT development, important steps have been accomplished to this direction, with the implementation of high performance academic and commercially available, generic and application targeted systems [2], [3], [4]. Moreover, significant research has been performed in the image reconstruction problem formulation and post-processing algorithms [1], [5]. However, EIT has not yet become widely applicable in medical equipment.

As a result, there is a lack of available EIT in-vivo data, relative to other imaging techniques, which is essential for

the validation of reconstruction algorithms, the determination of system standards, comparisons and even training Machine Learning structures that are currently gaining popularity in EIT applications [6], [7]. Recently, some notable efforts have been made for the classification of open-source EIT data; however, there is still a large field for new investigations [8].

Absence of medical data makes the usage of accurate simulation models necessary for the evaluation and testing of reconstruction approaches. Although numerous accurate F.E.M. structures have been utilized for many applications, in ventilation Time-Difference EIT (Td-EIT) imaging, most of them are actually reduced to two extreme states: full-inhalation and full-exhalation of the lungs ignoring all in-between instances [9], or changes during an individual frame measurement [5]. Furthermore, many of them do not consider the shape-changes of both the boundary (and hence the exact electrode positions) and the tissues during breathing. What actually happens in lung EIT monitoring is that each measuring frame needs a time interval to be recorded. During this space, both electrical and geometric properties are continuously changing. Therefore, for modest frame rates (< 30 fps), each set of measurements per frame can not be considered as an EIT "snapshot".

Hence, a thoracic-EIT simulation model which includes numerous shape, conductivity and permittivity states is essential for observing EIT images' behavior through various frame rates, correlated with other parameters such as the electrode number, bio-signal noise levels and measurement pattern. This view can lead to useful conclusions for both the design and the functional parameters of a ventilation-monitoring EIT system.

In this paper, a highly tunable, two-dimensional dynamic thoracic F.E.M. model is presented, which includes the following tissues: skin and fat, bones, lungs, muscle and heart. The electrodes' number and characteristics, structure geometry, breathing times and Heart Beat Rate (HR) as well as the Frames Per Second (FPS) and measuring strategy (skip protocol [10]) can be initially defined. Collapsing regions can also be defined. The time-variant model is implemented based on CT images by using MATLAB and FEMM software tools in the following way: a .lua script is created by a MATLAB code and executed in the FEMM software, where a particular shape, conductivity and permittivity state of the thorax is sketched at each time step. The shape and position states of all tissues except heart, are determined by the corresponding ventilation cycle states, while conductivity and permittivity

are specified by the superposition of ventilation and blood circulation cycles.

This paper is organized as follows. In section II, the model's parameters and properties are extensively described. In section III, the process performed for the model's execution and measurement collection is presented. Furthermore, in section IV, time evolution simulation results are displayed and compared for selected initial parameters. Finally, in section V, the conclusion is written.

II. EIT MEASUREMENT PRINCIPLES

Although different types of measuring techniques have been developed, the most conventionally used is the current skip- m , voltage skip- n protocol [10]. In a N -electrode EIT system, a bipolar AC current source is applied to two electrodes with a gap of m electrodes between them, while differential voltages are acquired from two other electrodes, at a distance of n electrodes between each other (tetrapolar measurement). After the voltage measurements are taken, the bipolar source is shifted to the next electrode pair and potentials are collected in a serial or parallel way. The process described above continues for all N current electrode pairs and is briefly demonstrated in Fig. 1.

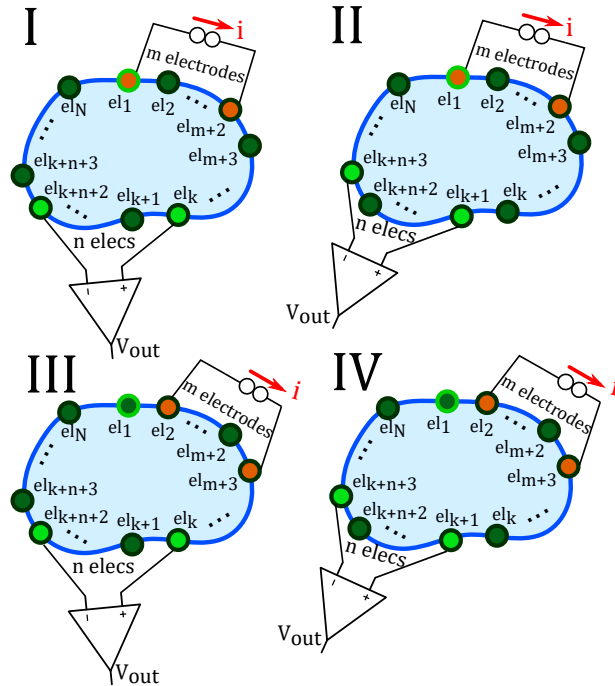


Fig. 1: Explanatory schematic of the current skip- m , voltage skip- n pattern. I: 1st current injection, voltage measurement between the k -th and $(k+n+2)$ -th electrodes (leaving a gap of n electrodes). II: Same current injection and next voltage measurement (between the $(k+1)$ -th and $(k+n+3)$ -th electrodes). III: Next current injection (source on 2nd and $(m+3)$ -th electrodes), voltage measurement between the k -th and $(k+n+2)$ -th electrodes. IV: Same current injection, next voltage measurement (between the $(k+1)$ -th and $(k+n+3)$ -th electrodes).

For each current electrode pair injection, $h = N - 3$ voltage measurements are acquired when $m = n$ or $h = N - 4$,

in case $m \neq n$. Therefore, for all current source positions, a total number of $N \cdot h$ voltage measurements is taken, which together create a single EIT measurement frame and are utilized in order to extract a static image through an inverse reconstruction algorithm. If f_r denotes the imaging frames per second (fps), then the total time needed for a frame is $t_{fr} = f_r^{-1}$. For our model, we assume that the time interval between two continuous current electrode-pair position changes is a discrete time step $t_{step} = t_{fr}/N$.

However, to compensate for modelling errors, differential frame imaging in time or frequency domains (Td-EIT or Fd-EIT) is extensively adopted [1], where an initial frame is utilized as reference. ventilation monitoring is one of the most widespread applications of Td-EIT, where L measurement frames are needed for the reconstruction of $L - 1$ images. Since the reference is usually the first frame, lung Td-EIT does not reveal the absolute conductivity distribution of the examined thoracic domain. Instead, it illustrates an estimation of the conductivity variations, compared to the first frame each time. This can provide temporal information for pulmonary operation over time which in these applications is more important than real conductivity values. The latter can be later approximated by applying appropriate a-priori data about the corresponding tissue conductivities.

III. MODEL STRUCTURE AND PARAMETERS

The two-dimensional thoracic model implemented represents a specific cross-section of the thorax. Although the actual thoracic geometry is three-dimensional and many 3D models have been utilized for EIT reconstruction algorithm evaluation [5], no models that include temporal tissue boundary and admittance behavior during particular frames exist in the literature. The development of a high temporal resolution model needs to be primarily in 2D due to the large numerical complexity of the problem, caused by continuous reshaping and remeshing.

A. Tissue Movement

The model described has a dynamic behavior during each EIT simulation. The boundaries of the skin and lung tissue, as well as the position of the chest-placed electrodes and bones (ribs and vertebra) are assumed to synchronously and gradually change between two initially defined constant states, due to the breathing process. The first one indicates the deflated (minimum air in lungs) condition while the second one denotes the fully inflated case (maximum air). The boundary deviation of the lungs is set larger than in the case of the ribs and electrodes' positions, while the number of discrete steps (total positions) between inhalation and exhalation is expressed by:

$$P = \frac{N \cdot t_{br} \cdot f_r}{2} \quad (1)$$

where t_{br} is the time needed for a single breath cycle.

Each model which describes tissue (except the heart), skin or electrode boundary consists of a time-variant n -polygon, represented by a point sequence $B_n(t) = [b_i(t)]$, where $i = \{1, 2, \dots, n\}$ corresponds to the i th point. We consider

that $B_n^{inh} = [b_i^{inh}]$ and $B_n^{exh} = [b_i^{exh}]$ are the initially defined boundary point positions at the exact times of inhalation and exhalation respectively. Each point $b_i(t) = (x_{bi}(t), y_{bi}(t))$ has a total deviation of $Dx_i = \|b_i^{inh} - b_i^{exh}\|$, and the corresponding space step during t_{step} is calculated by:

$$dx_i = \frac{Dx_i}{P} \quad (2)$$

which for the sake of simplicity is assumed to be time-proportional. Hence, dx_i denotes the shift $b_i(t_{j+1}) - b_i(t_j)$, with $t_{step} = t_{j+1} - t_j$ of a polygon's point b_i during the time that current is injected from a single electrode pair.

The heart tissue boundary can be described by a polygon point sequence $H_n(t) = [h_i(t)]$, where $i = \{1, 2, \dots, n\}$ also corresponds to the i th point. At the diastolic and systolic-end states the heart boundary polygon gets the following sequence values: $H_n^d = [h_i^d]$ and $H_n^s = [h_i^s]$. For each heart boundary polygon point, the total deviation is $Dh_i = \|h_i^d - h_i^s\|$ and the space step during t_{step} is given by:

$$dh_i = \frac{2Dh_i}{N \cdot t_{pulse} \cdot f_r} \quad (3)$$

where t_{pulse} is the duration of a single heart beat. The total positions of the heart boundary points can be calculated in the following way:

$$Q = \frac{N \cdot t_{pulse} \cdot f_r}{2} \quad (4)$$

It is noted that the heart tissues' deviation should be chosen relatively smaller than the lung tissues' one.

B. Admittance temporal behavior

During the pulmonary and cardiac cycles, apart from the tissues' shapes and positions, significant changes are also detected at most of the admittances.

The most intense variations take place in the lungs, where conductivity σ and permittivity ϵ depend on their volume and their air content. A less important change in both σ and ϵ is caused by blood flow in lungs. Thus, their admittance can be expressed as a function of the pulmonary and circulation cycle states each time.

To set the pulmonary-cycle related lung's admittance, we first assumed that each lung's relative volume F changes piecewise linearly with timesteps $1 \leq i \leq 2P$ during a single breathing period ($t_1 \leq t_i \leq t_{2P}$):

$$F_i = \begin{cases} \frac{3}{P+1}i + \frac{3}{P-1} + 4, & \text{if } 1 \leq i \leq P \\ -\frac{3}{P+1}i - \frac{6P+3}{P+1} + 4, & \text{if } P \leq i \leq 2P \end{cases}$$

This piecewise linear function here has been defined for simplicity, since the true dependence of air volume F from time is obviously more complex and might depend on each particular breath's characteristics. The air-related conductivity of a lung as a function of its air volume can be approximated by [11]:

$$\sigma_{l,air} = K_1 \left(\frac{0.85s_b}{w} + 0.03s_i \right) \frac{32F + 4.5}{(32F + 9)^2} + K_2 \quad (5)$$

Where s_b , w and s_i are parameters related with morphological lung properties [11] and are selected as $s_b = 0.5$, $w = 1.5$

and $s_i = 2$ (mean values). K_1 and K_2 are frequency related parameters and are properly chosen in order to scale $\sigma_{l,air}$ between the absolute inflated ($\sigma_{l,air}(f, F_{max})$) and deflated ($\sigma_{l,air}(f, F_{min})$) lung conductivity values for the used measuring frequency f , as given from [12], [13]. In case of the air-related lung permittivity, the following approximation has been performed [11]:

$$\epsilon_{l,air} = L_1 \left(\frac{0.85e_{rb}}{w} + 780F^{1/3}e_{rm} \right) \frac{32F + 4.5}{(32F + 9)^2} + L_2 \quad (6)$$

Where e_{rb} and e_{rm} are also morphological lung parameters, selected as 10000 and 10, respectively [11]. L_1 , L_2 scale the permittivity between the corresponding inflated and deflated values at the chosen frequency, defined in [12], [13]. The air-related lung admittance value is:

$$\gamma_{l,air} = \sigma_{l,air}(f, F) + j2\pi f \epsilon_{l,air}(f, F) \quad (7)$$

The lungs admittance variation due to blood circulation is assumed to be a piecewise linear function for $t_1 \leq t_j \leq t_{pulse}$:

$$\delta\sigma_{l,blood}^j = \begin{cases} \frac{\Delta\sigma_{bo}}{Q}j, & \text{if } 1 \leq j \leq Q \\ -\frac{\Delta\sigma_{bo}}{Q}j + \Delta\sigma_{bo}, & \text{if } Q \leq j \leq 2Q \end{cases}$$

Where $\Delta\sigma_{bo}$ refers to the initially defined total lung conductivity variation due to blood circulation (10 - 20 times lower than air-related changes, 0.005 - 0.01 S/m [9]). The corresponding relative permittivity change is defined as:

$$\delta\epsilon_{l,blood}^j = \begin{cases} \frac{\Delta\epsilon_{bo}}{Q}j, & \text{if } 1 \leq j \leq Q \\ -\frac{\Delta\epsilon_{bo}}{Q}j + 2\Delta\epsilon_{bo}, & \text{if } Q \leq j \leq 2Q \end{cases}$$

$\Delta\epsilon_{bo}$ refers to the initially defined total lung permittivity variation due to blood circulation (200 - 500 F/m [9]).

While pulmonary cycle is at state i , $1 \leq i \leq 2P$ and cardiac cycle at state j , $1 \leq j \leq 2Q$, we write the total admittance of each lung:

$$\gamma_l^{i,j} = \gamma_{l,air}^i + \delta\gamma_{l,blood}^j = \sigma_{l,air}^i + \delta\sigma_{l,blood}^j + j2\pi f(\epsilon_{l,air}^i + \delta\epsilon_{l,blood}^j) \quad (8)$$

The heart admittance is assumed to change periodically and piecewise linearly. Thus:

$$\sigma_{heart}^j = \begin{cases} \sigma_{ho} - \frac{\Delta\sigma_{ho}}{Q}j + \Delta\sigma_{ho}, & \text{if } 1 \leq j \leq Q \\ \sigma_{ho} + \frac{\Delta\sigma_{ho}}{Q}j - \Delta\sigma_{ho}, & \text{if } Q \leq j \leq 2Q \end{cases}$$

and

$$\epsilon_{heart}^j = \begin{cases} \epsilon_{ho} - \frac{\Delta\epsilon_{ho}}{Q}j + \Delta\epsilon_{ho}, & \text{if } 1 \leq j \leq Q \\ \epsilon_{ho} + \frac{\Delta\epsilon_{ho}}{Q}j - \Delta\epsilon_{ho}, & \text{if } Q \leq j \leq 2Q \end{cases}$$

where σ_{ho} and ϵ_{ho} are the base inner heart conductivity and permittivity (approximately 0.4-0.5 S/m and $5 \cdot 10^4$ F/m respectively [12], [13]), while $\Delta\sigma_{ho}$ and $\Delta\epsilon_{ho}$ refer to the conductivity and permittivity changes of the heart due to blood presence (fixed to 0.025 S/m and 2000 F/m respectively).

Near the heart boundary, the myocardium muscle is defined, which consists of a frequency depended conductivity [14]:

$$\sigma_{mc}(f) = 9 \cdot 10^{-8} \cdot f + 0.168 \quad (9)$$

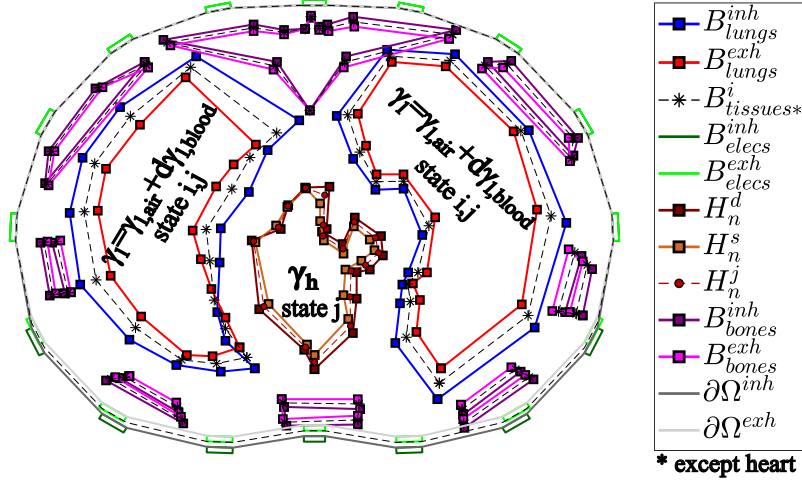


Fig. 2: Simplified sketch of the dynamic thoracic model. The inhalation and exhalation end, as well as the heart's systolic and diastolic end are noted. The shape boundaries are indicative, since they can be properly tuned. No collapsed areas and skin/fat are included for clarity.

and a permittivity of [14]:

$$\epsilon_{mc}(f) = 2.29 \cdot 10^5 \cdot (10^{-3}f)^{-0.95} \quad (10)$$

It is noted that due to blood circulation, when $|\delta\gamma_{l,blood}|$ is maximized, $|\delta\gamma_{heart}|$ is minimized. Furthermore, piecewise constant functions were selected instead of harmonic ones, because the actual admittivity spectrums exhibit more complex behavior than a single harmonic. The model's accuracy can be further improved using proper regression models, which is not a part of this work.

The muscle tissue, which exists between bones and lungs has a permittivity set in a similar way to γ_{heart} above. Nonetheless, 180° phase shift has been added, due to the circulation cycle behavior. Moreover, we defined $\delta\sigma_m = 0.01$, $\sigma_{mo} = 0.28$ (S/m), $\delta\epsilon_m = 900$ (F/m) and $\epsilon_{mo} = 13 \cdot 10^3$ (F/m) [12].

The skin-fat (a thin inner layer near the boundary) admittivity is assumed to be constant at very small values (i.e. less than 0.03 S/m) [12], [13].

C. Silent spaces and collapsed areas

At the end of each breath, after the exhalation-end, a small silent time-space usually follows, where no breath activity is recorded. This space is included in the dynamic model's behavior and can be defined between 0.3 and 1.5 seconds. When each silent space ends, a new breath cycle begins with the inhalation process.

Chronic clinical conditions of lungs, such as Acute Respiratory Distress Syndrome (ARDS) may cause inflammatory edema that induces regional collapses [15]. This practically means that lungs do not homogeneously function, with some areas not inducing sufficient air volume. This is modeled by inducing 4 possible collapse cases (proportional to the area of collapse) at the left lung and 3 possible cases for the right lung. The selected collapsed area's admittance is not affected by the ventilation cycle state, contrary to the rest of the corresponding lung.

TABLE I: 2-D Thoracic Model Parameters

| Parameter | Description |
|---------------------------|--|
| $\partial\Omega^{inh}$ | domain's boundary at inhalation |
| $\partial\Omega^{exh}$ | domain's boundary at exhalation |
| $B_n^{inh}, B \neq heart$ | tissue/electrode polygons at inhalation-end |
| $B_n^{exh}, B \neq heart$ | tissue/electrode polygons at exhalation-end |
| H_n^d | heart shape at end-diastolic phase |
| H_n^s | heart shape at end-systolic phase |
| t_{pulse} | pulse duration (secs) |
| t_{br} | breath duration (secs) |
| z_{elec} | electrode contact impedances (Ω) |
| d_{elec} | electrode width (cm) |
| γ_l | standard lung admittance (σ_l, ϵ_l) |
| $\Delta\gamma_{l,air}$ | total lung admittance variation due to the breath ($\delta\sigma_{l,air}, \delta\epsilon_{l,air}$) |
| $\Delta\gamma_{l,blood}$ | total lung admittance variation due to the HR ($\delta\sigma_{l,blood}, \delta\epsilon_{l,blood}$) |
| γ_{ho} | standard heart admittance ($\sigma_{ho}, \epsilon_{ho}$) |
| $\Delta\gamma_{ho}$ | total heart admittance variation due to the HR ($\Delta\sigma_{ho}, \Delta\epsilon_{ho}$) |

D. Electrode modelling

The electrodes are modelled as rectangular 2D shapes, with an adjustable width d_{elec} . Their contact impedance relative to area, is approximated by the following formula:

$$\rho_{elec} = Z_{elec} \frac{S}{d_{elec}} \quad (11)$$

where Z_{elec} is the electrode's contact impedance and S the corresponding surface area.

IV. EXECUTION PROCESS

The process begins with the initialization of the total tissue and electrode positions, as well as their admittance properties in the time domain, according to the model and measurement input parameters. A .lua script is opened and processed via MATLAB and time-constant properties (bone conductivity and

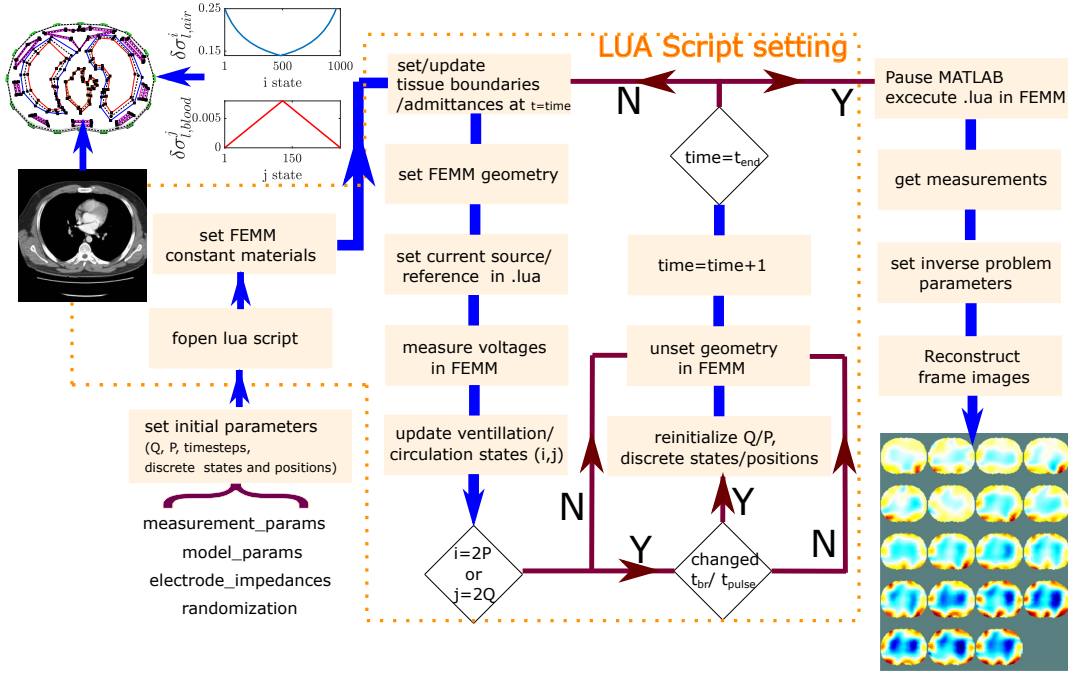


Fig. 3: Explanatory diagram of the process performed for the temporal thoracic model execution in FEMM and the measurement collection from MATLAB.

permittivity, collapsed areas, e.t.c.) are set. It is also noted, that the input domain's boundary ($\partial\Omega^{inh}$ and $\partial\Omega^{exh}$), as well as the tissues' respiratory end boundaries (B_n^{inh} and B_n^{exh}) are derived from a CT scan [16], considering a lung volume change of 15% and chest movement of 1 cm (5% vertical change) [5]. The user can also choose to randomize all boundaries, with a standard deviation of 5%. Both initial ventilation and circulation states can also be randomly selected.

For each discrete time step (i.e. current injection, see section II), the tissue current positions and admittances are updated according to the pre-defined sequence (see 1st step). FEMM is instructed to construct the corresponding structure and perform voltage measurements on the electrodes. Furthermore, both ventilation and circulation states are checked. When a breathing cycle ends, a silent space begins that lasts up to 1 second. If a silent space has ended, a new breath cycle begins, with a duration that differs from the previous one at a maximum of 20%. Then, P is recomputed and the tissues' discrete positions and temporal admittances are redefined according to equations (1), (2) and (7). In addition, every 3 circulation cycles, HR changes randomly at a maximum of 2% (assuming calm patient state). In this case, Q , heart tissue discrete positions and each tissue's blood-cycle related admittance variation in time are redefined according to (3), (4) and the piecewise linear functions defined in section II. The updates and checks described are repeated until the final time step simulation t_{end} is reached.

When the loop is exited, a .lua script is created and MATLAB pauses in order to execute the script using the FEMM software. The latter automatically follows the steps

TABLE II: Measurement Parameters

| Parameter | Description |
|-----------|---|
| N | Number of electrodes |
| f | Current signal frequency (Hz) |
| I | Current signal amplitude (mA) |
| m | Current skip-pattern |
| n | Voltage skip-pattern |
| n | Voltage skip-pattern |
| n | Voltage skip-pattern |
| t_{fr} | Time needed for each frame (fps^{-1}) |
| t_{end} | Total simulation time (secs) |

written in the .lua file, efficiently recreating and remeshing the structure at each time step. Electrode potential measurements are written in text files, which are then parsed and assembled by MATLAB according to the selected measuring pattern. Finally, measurements are utilized as inputs to an inverse reconstruction algorithm, where proper hyperparameters are selected.

The process flow is demonstrated in Fig. 3 and the previously selected measurement parameters are presented in Table II. The code written for this development is available under an open-source license at <https://github.com/chdim100/Dynamic-Thoracic-Model-for-EIT>.

V. SIMULATIONS AND RESULTS

To evaluate the proposed simulation model, a number of simulation cases were derived. In particular, $N = 16$ and $N = 32$ electrodes are selected for simulation test cases of 6 second duration. Imaging is performed at 5, 10 and 30 fps for a current frequency of $200kHz$. During each

frame, the shape and admittance properties of each tissue are dynamically changing, as described in previous sections. The current *skip* = 2 measuring protocol is used in the 16-electrode simulations, while for the 32-electrode cases we selected the current *skip* = 4 pattern. In both electrode cases, differential voltages are measured from adjacent electrode pairs (voltage *skip* = 0).

The model parameters are initialized as follows: the inspiration and expiration end positions are defined according to a specific CT scan (where boundaries are used as mid-points) [16]. The shapes are not further processed via randomization. In order to get clear comparisons, initial breath time is set to 3 seconds, while silent space is set to 0.3 seconds (non-random). Within the 4th second of the simulation, a 2nd breath cycle begins, which has a duration of 3.6 seconds (increased by 20%) and is not completed until the simulation ends. The *HR* is 75 bpm for the first 3 beats, and then increases to 77.25 bpm (+3% increment). The right lung is assumed to be healthy, while a lung collapse that corresponds to the 20% of the total left lung's modeled area is inserted. The whole time-evolution of each dynamic tissue's impedance is demonstrated in Fig. 4.

The electrodes are assumed to have a width of $d = 0.5$ cm and relative conductivities with a mean value of 0.02 (S/m) and 15% standard deviation, since in real EIT cases, contact impedances always have a variation [17]. The values above are computed using (11), assuming $E[z_{elec}] = 1k\Omega$ (dry electrode at 200 kHz for long-term monitoring [18]).

The FEMM time-variant F.E. model includes $\sim 7000 - 7500$ nodes and $\sim 12000 - 14500$ elements, dependent on the number of the electrodes and the boundaries state. Remeshing is performed at each discrete time step (which as referred corresponds to a bipolar current source position).

For the time-differential image reconstructions, the Gauss-Newton iterative algorithm has been evaluated. The relative conductivity (or admittance) estimation problem can be described as minimization of the following expression [1]:

$$\underset{\delta\sigma}{\operatorname{argmin}}\{\|J\delta\sigma - \delta V\|_W^2 + \lambda^2 \|\delta\sigma\|_Q^2\} \quad (12)$$

Where $\delta\sigma$ is the conductivity change under estimation, δV the electrode-measured differential potentials, J the Jacobian matrix around a linearization point $\sigma = \sigma_o$, which actually indicates the potential field's sensitivity to conductivity changes. W is a weight matrix, used for calibrating the imbalanced electrode contacts, λ a regularization hyperparameter and Q a prior filter matrix [1]. The function under minimization includes a least-square term and a penalizing regularization term ($\|\delta\sigma\|_Q^2$), in order to encounter the problem's ill-posedness and ill-conditioning [1].

The imaging process is performed in MATLAB using the EIDORS library tool [8]. Reconstructions take place on a default EIDORS static thorax-shape F.E. model, which contains 1024 elements. The hyperparameter is heuristically selected $\lambda = 0.25$ for the 16-electrode cases and $\lambda = 0.03$ for the 32-electrode cases. In addition, Gaussian noise has been added so that the simulated measurements for all cases have a 50 dB SNR which is a moderate noise level for ventilation EIT

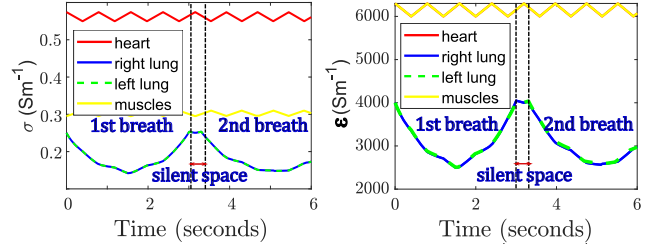


Fig. 4: Temporal tissues admittances defined for the simulation (200 kHz). Heart and muscle tissue permittivities are almost equal.

measurements [7]. It is noted that for high frame rate levels, averaging which increases the signal's SNR is not possible, hence reducing the frame rate level is often preferred for SNR optimization [3]. However, lower fps levels obscure significant temporal information about both ventilation and cardiac-related functions. In order to examine the way lower noise reduces spatial imaging artifacts, a 65 dB SNR signal case has been added for the lower frame rate test cases (5 and 10 fps).

The time evolution of the reconstructed images for 16 and 32 electrodes and each frame rate and noise testcase is shown in Fig. 5. Furthermore, to get quantitative information and a clearer comparison of the images' temporal behaviors, we have segmented 3 constant Regions of Interest (ROIs) in the inverse reconstruction model (Fig. 6 VI). The first two regions correspond to the areas considered as lungs while the third demonstrates the heart tissue's area. For each ROI, the mean estimated conductivity values over its elements are computed and displayed in the time domain in Fig. 6 (I-V).

In all cases, the breathing activity is successfully detected, since two large conductivity curve "valleys" appear in ROIs I and II (Fig. 6). Their behavior follows the lung admittance evolution shown in Fig. 4. In both the 16 and 32 electrodes configurations, when imaging at low fps (5 - 10) the contribution of the SNR's increase from 50 to 65 dB is observable, since the images' artifacts are decreased, and the curves in Fig. 6(I-IV) are smoother, appearing less intense random variations. Increasing the fps rate, leads to acquiring more information about some details that can be utilized for further functional analysis [19], [20]. In addition, higher frame sampling gives a more reliable data for each breath's exact depth (i.e. in this example the two breaths are equal, however this is detectable only for $f_{fr} > 10$ fps, as observed in Fig. 6). At 30 fps, the imaging quality difference between 16 and 32 electrodes is clear, where in the latter, the left lung's collapsed area is detected without any post image processing (the left lung's impedance change area size is significantly lower than the right ones). The lung, muscle and heart's temporal behaviors due to the blood cycle are still not noticeable without further time and frequency domain analysis, however, for 30 fps some higher frequency periodicity in ROI III can be slightly observed in Fig. 6 V.

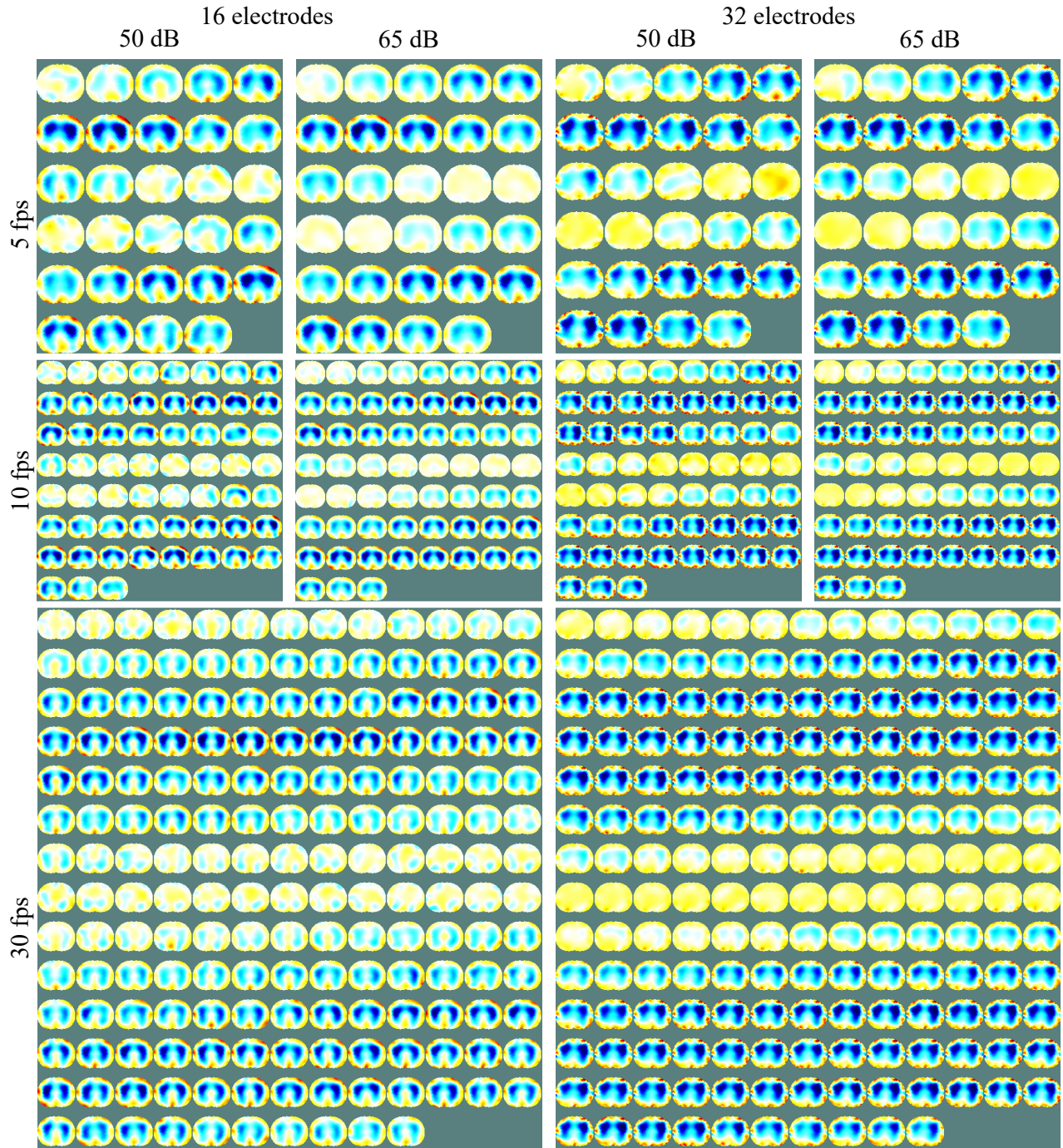


Fig. 5: EIT image reconstruction of 2 breath cycles of the simulated dynamic model. The first column shows the 16-electrode configuration images, while the second column depicts the 32-electrode case. Each sub-case is displayed in a particular gray frame. When the lungs are in deflated state, the impedance changes are very low, since at all the performed simulations, the reference frame corresponds to full-exhalation end. While the exhalation process takes place, the lung area's impedance gradually decreases (darker blue colors), until it reaches the full-inflated state. From this point the lung impedance begins to increase again and the exhalation part takes place. In order to distinguish the differences between the cases temporal resolution, all the frames are figured.

VI. CONCLUSION

A high temporal resolution multiparameter thoracic simulation model for EIT was described in this paper. The

simulations are executed in MATLAB and FEMM software. The effect of ventilation (breathing) and circulation (blood) cycles on tissue movement and admittances was taken into

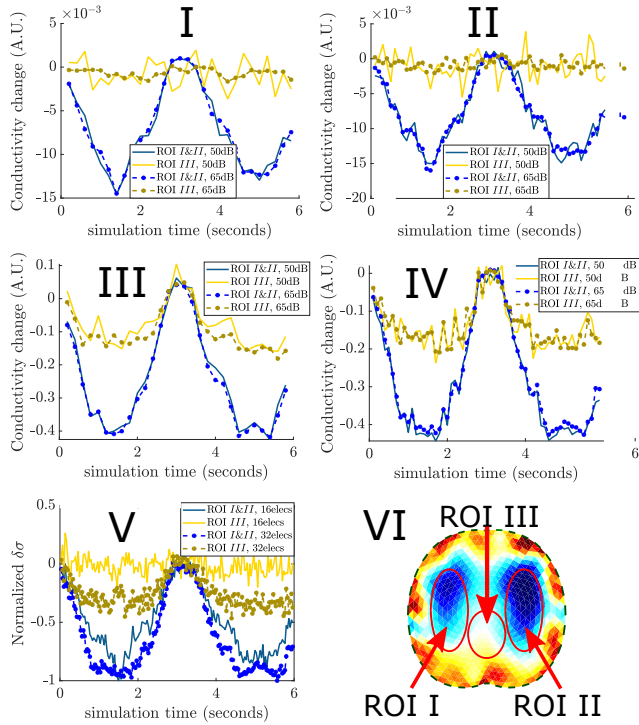


Fig. 6: Mean estimated (arbitrary) values of each ROI over the time. Case I: 16 electrodes, 5fps. Case II: 32 electrodes, 5fps. Case III: 16 electrodes, 10 fps. Case IV: 32 electrodes, 10 fps. Case V: 16 and 32 electrodes while imaging at 30fps. VI: the 3 ROI areas, related to the inverse reconstruction model.

account during each frame measurement. For each frame, the bipolar current source is shifted N times between the electrodes and each one is considered as a discrete simulation time step, giving a resolution of N time steps per frame. The simulation model's tunability can be further improved, with the randomization of more thoracic sections and chest-types initial boundaries. Extensive functional analysis and post processing needs to be performed on the images, in order to acquire valid medical data.

ACKNOWLEDGMENT

This research is co-financed by Greece and the European Union (European Social Fund- ESF) through the Operational Programme "Human Resources Development, Education and Lifelong Learning" in the context of the project "Strengthening Human Resources Research Potential via Doctorate Research" (MIS-5000432), implemented by the State Scholarships Foundation (IKY).

REFERENCES

[1] A. Adler and A. Boyle, "Electrical Impedance Tomography: Tissue properties to image measures," *IEEE Transactions on Biomedical Engineering*, vol. 64, no. 11, pp. 2494–2504, 2017.

[2] Y. Wu, D. Jiang, A. Bardill, R. Bayford, and A. Demosthenous, "A 122 fps, 1 MHz bandwidth multi-frequency wearable EIT belt featuring novel active electrode architecture for neonatal thorax vital sign monitoring," *IEEE transactions on biomedical circuits and systems*, vol. 13, no. 5, pp. 927–937, 2019.

[3] M. M. Mellenthin, J. L. Mueller, E. D. L. B. de Camargo, F. S. de Moura, T. B. R. Santos, R. G. Lima, S. J. Hamilton, P. A. Muller, and M. Alsaker, "The ace1 Electrical Impedance Tomography system for thoracic imaging," *IEEE Transactions on Instrumentation and Measurement*, vol. 68, no. 9, pp. 3137–3150, 2018.

[4] H. Wi, H. Sohal, A. L. McEwan, E. J. Woo, and T. I. Oh, "Multi-frequency Electrical Impedance Tomography system with automatic self-calibration for long-term monitoring," *IEEE transactions on biomedical circuits and systems*, vol. 8, no. 1, pp. 119–128, 2013.

[5] D. Liu, V. Kolehmainen, S. Siltanen, A.-M. Laukkanen, and A. Seppänen, "Nonlinear difference imaging approach to three-dimensional Electrical Impedance Tomography in the presence of geometric modeling errors," *IEEE Transactions on Biomedical Engineering*, vol. 63, no. 9, pp. 1956–1965, 2015.

[6] S. J. Hamilton and A. Hauptmann, "Deep D-bar: Real-time Electrical Impedance Tomography imaging with deep neural networks," *IEEE transactions on medical imaging*, vol. 37, no. 10, pp. 2367–2377, 2018.

[7] Z. Wei and X. Chen, "Induced-Current learning method for nonlinear reconstructions in Electrical Impedance Tomography," *IEEE transactions on medical imaging*, 2019.

[8] A. Adler and W. R. Lionheart, "Uses and abuses of EIDORS: an extensible software base for EIT," *Physiological measurement*, vol. 27, no. 5, p. S25, 2006.

[9] V. Tomicic and R. Cornejo, "Lung monitoring with Electrical Impedance Tomography: technical considerations and clinical applications," *Journal of thoracic disease*, vol. 11, no. 7, p. 3122, 2019.

[10] O. L. Silva, R. G. Lima, T. C. Martins, F. S. de Moura, R. S. Tavares, and M. S. G. Tsuzuki, "Influence of current injection pattern and electric potential measurement strategies in Electrical Impedance Tomography," *Control Engineering Practice*, vol. 58, pp. 276–286, 2017.

[11] P. Nopp, E. Rapp, H. Pfitzner, H. Nakesch, and C. Rusham, "Dielectric properties of lung tissue as a function of air content," *Physics in Medicine & Biology*, vol. 38, no. 6, p. 699, 1993.

[12] S. Gabriel, R. Lau, and C. Gabriel, "The dielectric properties of biological tissues: II. measurements in the frequency range 10 Hz to 20 GHz," *Physics in medicine & biology*, vol. 41, no. 11, p. 2251, 1996.

[13] —, "The dielectric properties of biological tissues: III. Parametric models for the dielectric spectrum of tissues," *Physics in Medicine & Biology*, vol. 41, no. 11, p. 2271, 1996.

[14] K. Raghavan, J. E. Porterfield, A. T. Kottam, M. D. Feldman, D. Escobedo, J. W. Valvano, and J. A. Pearce, "Electrical conductivity and permittivity of murine myocardium," *IEEE Transactions on Biomedical Engineering*, vol. 56, no. 8, pp. 2044–2053, 2009.

[15] M. C. Bachmann, C. Morais, G. Bugedo, A. Bruhn, A. Morales, J. B. Borges, E. Costa, and J. Retamal, "Electrical Impedance Tomography in acute respiratory distress syndrome," *Critical Care*, vol. 22, no. 1, pp. 1–11, 2018.

[16] H. M. Orozco, O. O. V. Villegas, V. G. C. Sánchez, H. d. J. O. Domínguez, and M. d. J. N. Alfaro, "Automated system for lung nodules classification based on wavelet feature descriptor and support vector machine," *Biomedical engineering online*, vol. 14, no. 1, p. 9, 2015.

[17] E. Demidenko, A. Borsic, Y. Wan, R. J. Halter, and A. Hartov, "Statistical estimation of EIT electrode contact impedance using a magic Toeplitz matrix," *IEEE transactions on biomedical engineering*, vol. 58, no. 8, pp. 2194–2201, 2011.

[18] R. Kusche, S. Kaufmann, and M. Ryschka, "Dry electrodes for bioimpedance measurements—design, characterization and comparison," *Biomedical Physics & Engineering Express*, vol. 5, no. 1, p. 015001, 2018.

[19] I. Frerichs, M. B. Amato, A. H. Van Kaam, D. G. Tingay, Z. Zhao, B. Grychtol, M. Bodenstein, H. Gagnon, S. H. Böhm, E. Teschner *et al.*, "Chest Electrical Impedance Tomography examination, data analysis, terminology, clinical use and recommendations: consensus statement of the TRanslational EIT developmeNt stuDY group," *Thorax*, vol. 72, no. 1, pp. 83–93, 2017.

[20] C. Putensen, B. Hentze, S. Muenster, and T. Muders, "Electrical Impedance Tomography for cardio-pulmonary monitoring," *Journal of clinical medicine*, vol. 8, no. 8, p. 1176, 2019.